Chapter 7

Laser and Hybrid Laser-Arc Welding

G. A. Turichin

Additional information is available at the end of the chapter

http://dx.doi.org/10.5772/64522

Abstract

Laser and hybrid laser-arc welding are used at present in modern industry, having many advantages over traditional welding technology. Sectors such as the automotive industry, shipbuilding, aviation and space industry, chemical machinery, defense industry, and so on cannot be imagined without these technologies. Possibility of dramatic increase of weld joint properties, robustness, and high level of process automation makes the technology of laser and hybrid material processing a prospective part of the industry. At the same time, physical complexity of these processes, their cross-science nature, and necessity in high-level skilled stuff require many efforts for wide and successful industrial implementation. Present manuscript, devoted to discussion of physical peculiarity of laser and hybrid laser-arc welding of metals, approaches to physical-based design of technological equipment, as well as examples of industrial applications of laser and hybrid welding concerning the possibility to control welded metal structure and properties, is one of the steps on this way.

Keywords: laser, welding, laser material processing, hybrid welding, laser-induced plasma, technological equipment, process control, process monitoring, kinetics of phase transformations

1. Introduction

There is a tendency of modern industry to decrease construction weight that is connected to the necessity of increasing fuel efficiency. For this purpose, new high-strength, two- and three-phase steels are applied, as well as new Al- and Ti-based alloys, and their properties are defined by parameters of inclusions ensembles. New technologies for automotive bodywork use tailored blanks when the welded blanks are exposed by stamping. Weight reduction blanks with the same mechanical characteristics are possible by using new high-strength steels. Nevertheless,

there is the problem of providing required characteristics of welds. It is also important to minimize welding stress and distortion, provide quality assessment, and process automation.

For these problems to be solved, intensive development and wide industrial implementation of laser and hybrid laser-arc welding (HLAW) becomes necessary in near future. Having a lot of evident advantages, beam welding due to complicity of technological processes needs to be successfully used with a deep understanding of process peculiarities, new CAE-based approaches of technology design, design of technological equipment on the basis of high brightness fiber lasers, technical vision, and process monitoring, as well as creation of new classes of welding materials.

Use of laser radiation and electric arc together for welding of metals and alloys so that both sources of heating influence on a material within just one heating zone was born 30–35 years ago [1]. Until recently, CO_2 lasers with radiation in far-infrared region were used. Metal interaction with the laser radiation of 10.6 and 1.06 μm is principally different. Lasers with such wavelength radiation are of poor quality and low accuracy. Only in recent years continuous fiber power lasers with good quality has been developed. They possess high beam quality and high accuracy.

Hybrid laser-arc welding is one of the most promising technologies for joining thick and heavy parts for production of gas and oil pipes, shipbuilding industry, building constructions, and bridge sections. The main benefit of hybrid laser-arc welding is the possibility to weld by one path materials with thickness of up to 20 mm and more, including new type of steels and modern alloys. Hybrid welding can also provide high-quality weld seam whose properties are comparable with laser weld seam properties, but the use of this technology in the case of real production is restricted by high complicity of the process [2] and appearance of different defects, such as porosity, cracks, spiking, and humping in the weld seam.

The analysis of results of the carried investigations of hybrid laser-arc welding process enables to determine the series of problems, in which decision is needed to develop reliable welding technology of thick metals and alloys. It is necessary to exclude: an undesirable direction of crystals growth; dramatic increase of the seam width in the top part of its cross-section; existence of hardening structures in deep penetration zone; presence of set of gas pores; and inadequate values of impact strength of the axial zone, notably at negative test temperatures. The overview of modern trends and problem for solution is presented in [3]. The only way to develop a reliable technology of hybrid laser-arc welding is the use of computer engineering-based approach to determine and optimize technological parameters as well as for finding and testing of technological methods.

2. Theoretical base of laser and hybrid welding

For understanding the weld pool formation and behavior during hybrid laser-arc welding it is comfortable to use two process models: first, for steady-state case, and second, for dynamic behavior of melt pool. The steady-state model is described in more detail in [4]. All incomplete

http://dx.doi.org/10.5772/64522

models consider main peculiarities of interconnected physical processes. Problem with laser beam absorption and reflection inside the keyhole, heat transfer in solid face, and task about vapor flow in keyhole are solved by the same way as it was done in the model of laser welding [4]. The arc and plasma models, which use boundary layer approximation for mass, momentum, current, and energy equations [5], are very specific for laser-arc welding. Media compressibility, volumetric heating by laser beam and arc current, mixing of metal vapor, shielding and arc gas, and temperature influence on kinetic coefficients have to be considered as well as workpiece surface influence on arc and shielding gas flow. The hybrid electric discharge, which defines values of ionization rate, and spatial distributions of conductivity and thermal diffusivity, is also very specific. Physical nature of listed processes is also important for the formation of melt pool, so it is necessary to look into it more deeply.

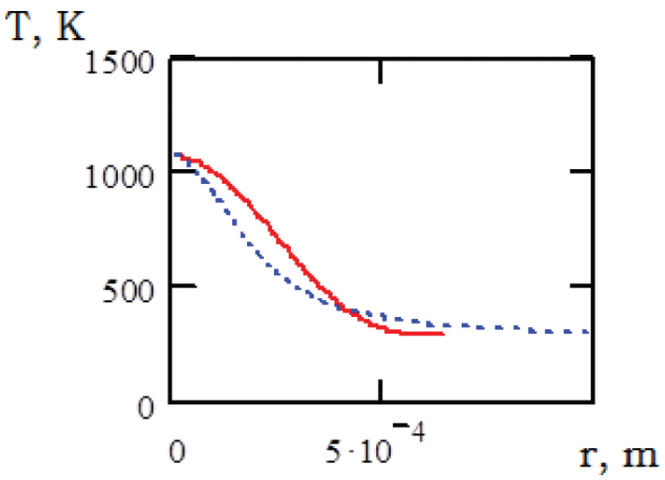

Figure 1. Jet radial temperature distribution 1 cm above surface, solid line – compressible gas, dot line – oncompressible.

The laser-induced plasma plume above the workpiece surface have an influence on welding process due to laser radiation absorption and refraction [6], and also can be used as an information source for online process monitoring [7] and control. As it is well known plasma plume structure and parameters are strongly dependent on radiation wavelength [8] and shielding gas nature and rate [9]. From the gas dynamics point of view, plasma plume is a subsonic submerged jet [10] of metal vapor in shielding gas with volumetric heating due to laser radiation absorption in the plasma. The numerical schemes [11] or well-known analytical solution for noncompressive submerged jet [12] are usually applied for calculation of the parameters of vapor-jet plasma. The volumetric heating, strongly influencing on jet flow, depend on plasma absorption coefficient. The theoretical descriptions of laser-induced plasma are usually supposed as thermodynamic equilibrium. The temperature of equilibrium plasma is defined ionization degree and others plasma parameters [13]. However, because absorption of radiation energy by plasma electrons and energy transfer from electrons to heavy component require an energy gap between light and heavy plasma components, supposition of thermodynamic equilibrium is not correct [14]. So the description of laser-induced plasma and also of plasma combined laser-arc discharge is to be based on solution of a Raiser kinetic

equation [15] for electrons energy spectrum, like it was done for laser-induced plasma in the keyhole [14], taking into account the chemistry and gas dynamics of plasma plume.

The analytic description of plasma plume in vapor-jet shielding gas mix with consideration of volumetric heating, heat conductivity, diffusion, viscosity, and compressibility effects for laser and hybrid welding is possible to get by means of application of boundary layer approach for plume gas dynamics and approach of physical kinetic for plasma of laser-arc discharge [5].

Enthalpy of vapor-gas mixture in plasma plume according to [5] in this case is given by the formula:

$$h = \left[\left(\frac{\nu\beta\left(1+B(x)\right)}{x} \frac{\chi/2\nu}{1-\chi/2\nu} - \frac{\alpha^2 PmC_p}{2\eta k x^2} \frac{r^2}{2} \right) \frac{1-\chi/2\nu}{\frac{\chi}{2\nu}\left(\frac{\nu\beta\left(1+B(x)\right)}{x}\right)^{\chi/2\nu}} \right]^{\frac{1}{1-\chi/2\nu}} \quad (1)$$

where r and x are the polar coordinates, constants α and β are given by initial conditions of momentum and energy fluxes [5], $B(x,\ y)=\int_0^x \frac{Q(x',\ y)\gamma}{h_c(x',\ y=0)\cdot h^*} dx'$, h_c is the initial value of vapor enthalpy, h^* is the vapor enthalpy for evaporation temperature, c is the heat capacity, Q is given by the formula $q=\frac{4m_e c\rho}{\sqrt{\pi}M_{Fe}M_{He}^2}\cdot\frac{v_\infty^2}{N_\infty^2\alpha_{Fe}}\cdot J_{Fe}\exp\left(-\frac{J_{Fe}}{\langle\varepsilon\rangle}\right)=Q\frac{c}{h}$, $q=\mu I$, I is the laser beam intensity, μ is the plasma absorption factor, η and ν are the dynamic and kinematic gas viscosity, and χ is the temperature diffusivity.

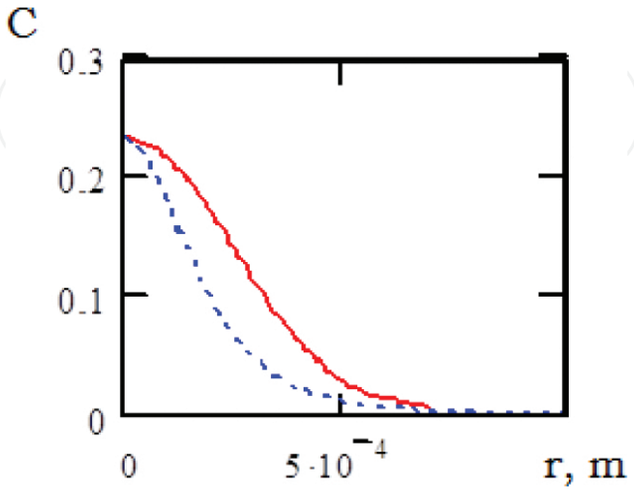

Figure 2. Iron concentration field in jet 1 cm above surface, solid line – compressible gas, dot line – non-compressible.

http://dx.doi.org/10.5772/64522

Figures 1–3 show examples of calculated distributions of temperature, mix density, and concentration in the plasma plume during laser welding of mild steel with initial temperature of 3200 K, flowing out of the keyhole with initial speed of 200 m/s into the helium shielding atmosphere of room temperature.

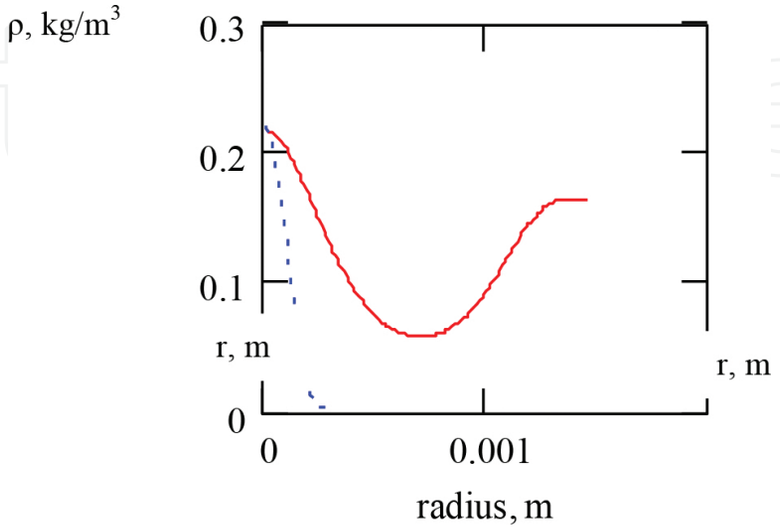

Figure 3. Density distribution on keyhole outlet, solid line – total density, dot line – iron vapor density.

The plasma plume interferometry experiments (**Figure 4**), made with the Michelson scheme, confirm the developed theory.

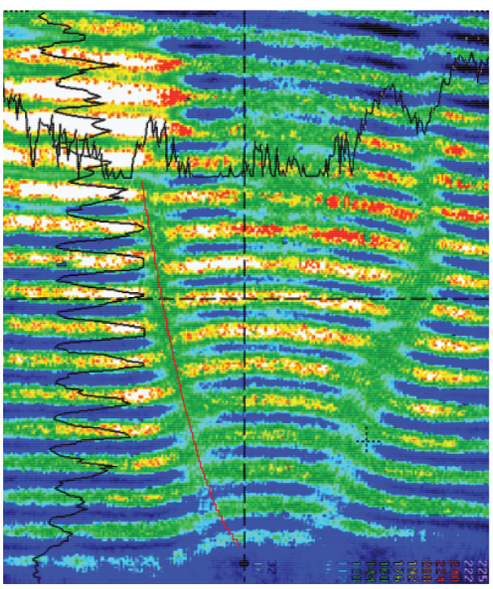

Figure 4. Plasma plume interferogram with calculated boundary of the jet (red solid line) for NdYAG laser welding.

Plasma plume volumetric heating due to laser beam absorption and Joule heating of electric arc make strong effect on parameters of plasma plume. Calculation shows that volumetric

heating due to plasma absorption lead to increases of jet thickness (**Figure 5**). The same behavior is typical for velocity and concentration (**Figure 6**) distributions. In calculation, the beam parameters which are typical for welding with deep penetration by CO_2 laser: beam power $W = 6$ kW, wavelength is 10.6 μm, focal radius $rf = 0.23$ mm, target material = mild steel, and shielding gas = He. The keyhole outlet radius (0.35 mm), initial jet velocity (200 m/s), and temperature (3200 K) were calculated by the simulation software LaserCAD [16].

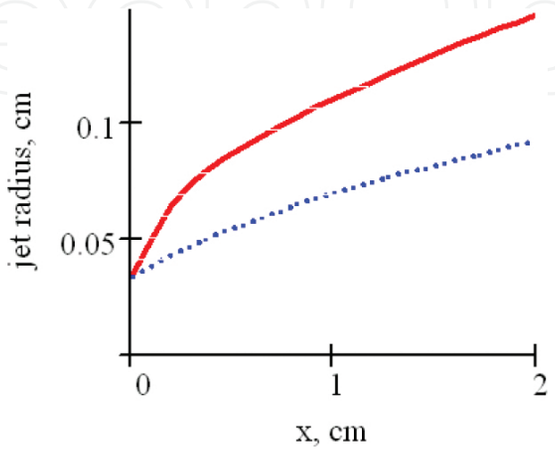

Figure 5. Boundary of the jet, solid line – with plasma absorption, dot line – without.

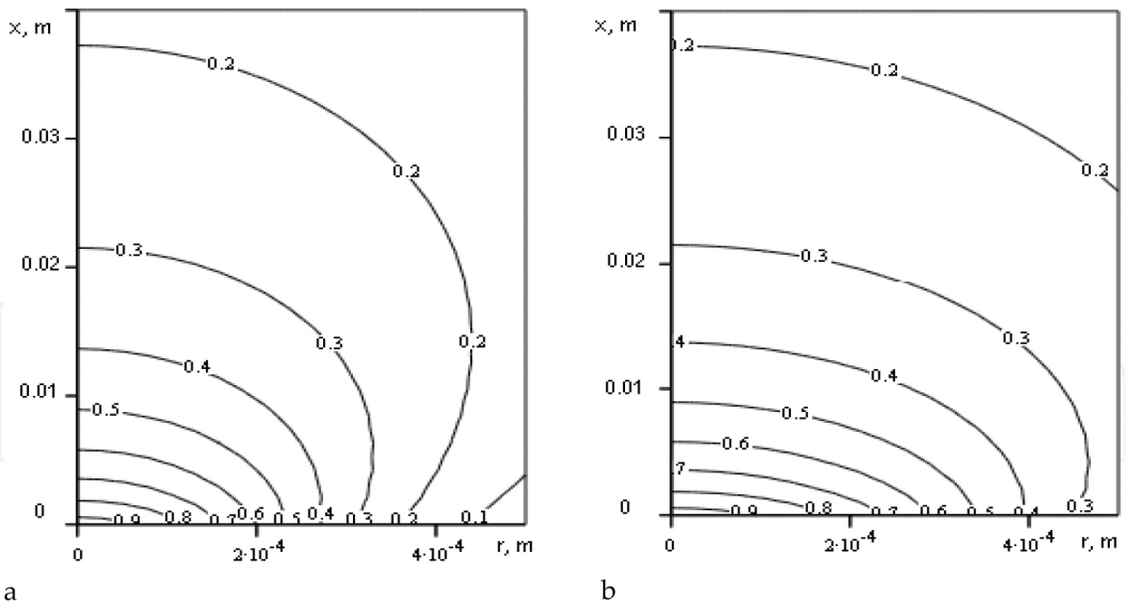

Figure 6. Distribution of metal vapor concentration in plasma plume, (a) without plasma absorption, (b) with consideration of plasma absorption.

Influence of plasma absorption with concurrence of heat convection with jet velocity and conduction in radial direction in plasma plume can shift a temperature maximum from the workpiece surface, even in the surface focusing (**Figures 7** and **8**). Also the difference between

http://dx.doi.org/10.5772/64522

the temperatures of electron and heavy plasma components, which characterize the plasma nonequlibrity, changes along the plume.

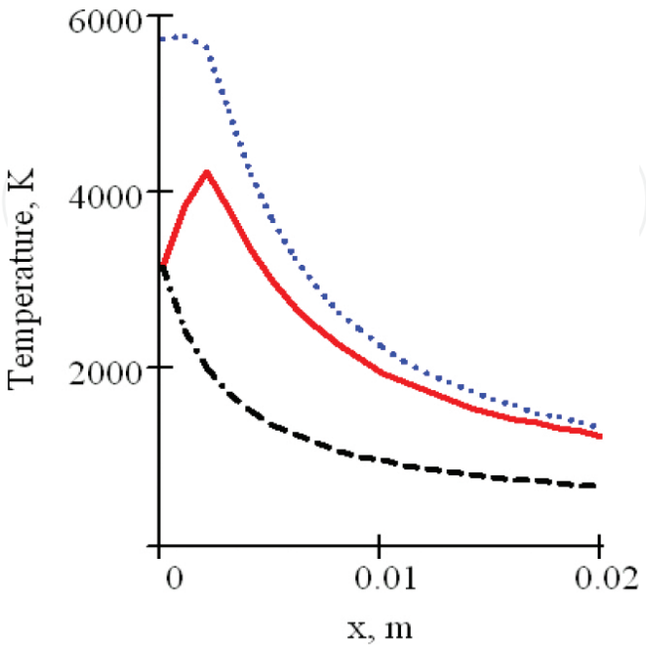

Figure 7. Temperature distribution along the plume axis, dot line – electron temperature, vapor-gas mix temperature – solid line – with, double dot – without plasma absorption.

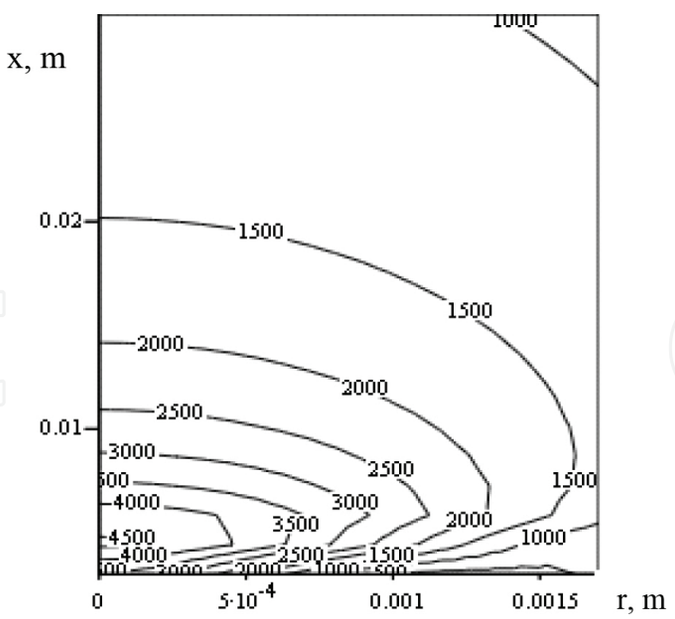

Figure 8. Temperature distribution in plasma plume.

Fast mixing of metal jet with surrounded gas limit the conductive kern formation by the region near the workpiece surface, as shown in **Figure 9**.

So, it is possible to mark that boundary layer gas dynamic model with consideration of discharge kinetics allow to explain an electric arc compression during hybrid welding by conductive kern formation in the near-surface region. The results of calculation also allowed to explain a shift of plume maximum temperature from the workpiece surface, which is often visible experimentally, not by the beam over focusing, but by the concurrence of heating with convection and conduction heat transfer.

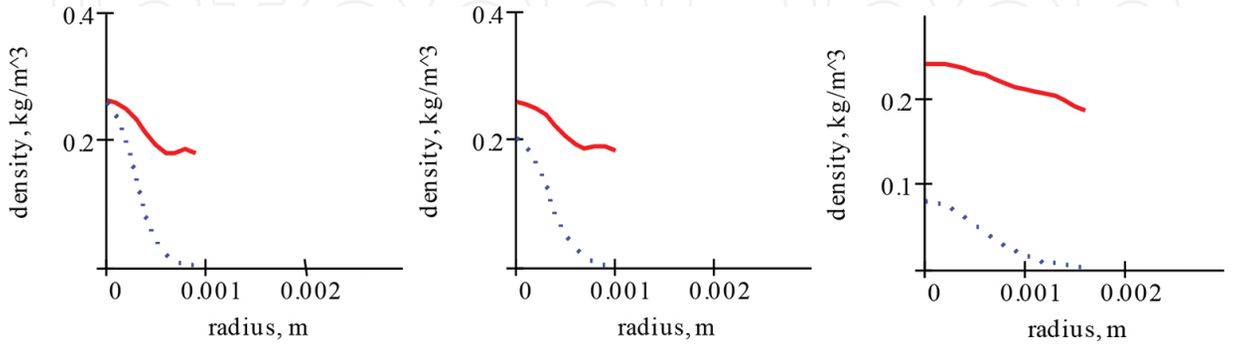

Figure 9. Radial distribution of mix density (solid) and metal density (dot) on the keyhole outlet and on the distances, correspondingly 0.3 and 2 cm.

Another specific problem for laser-arc welding in the case of laser-MAG and laser-MIG technology is a problem of filler wire melting. This problem can be described on the basis of one-dimensional approach with consideration of Stephan conditions on solid-liquid interface and the action of the electric force for drops transferring [17]. For solution of melt flow and heat transfer task in the melt pool, the approximation of potential flow of ideal liquid with viscous boundary layers on the melting front and keyhole surface has been used [4]. Because hybrid welding is often used for the welding of large and heavy parts, influence of gap between parts becomes especially important for this case.

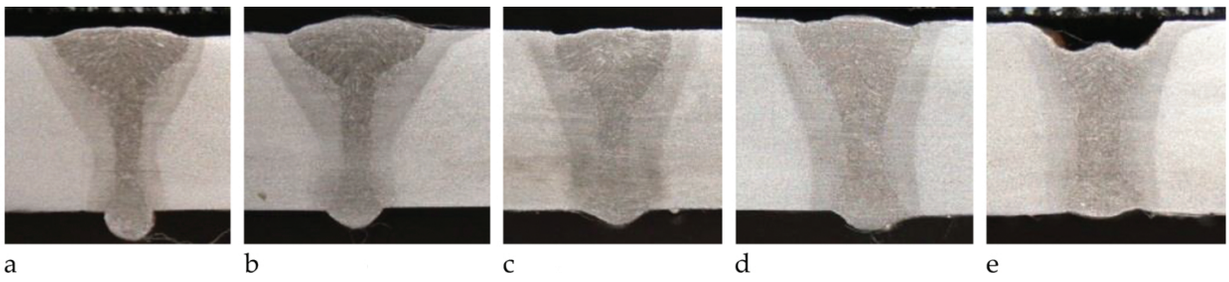

Figure 10. Weld macrosections with different gap width: a – 0 mm; b – 0.3 mm; c – 0.6 mm; d – 0.9 mm; e – 1.2 mm.

For most tasks of welding sheets and pipes, gap width influence on the quality of welding is important. In this area a large amount of research was carried out [18]. The authors found a reduction of the tensile strength and the destruction of the HLAW sample in the HAZ [19]. Experiments show that the highest efficiency and deepest penetration of alloy elements of the welding wire at the HLAW also depend on gap width [20]. Good weld appearance was created

http://dx.doi.org/10.5772/64522

at the HLAW of the low alloy high-strength steel with thickness of 16 mm with a various gap widths from 0 to 0.7 mm [21].

Experiments show that gap width makes an effect not only on weld formation stability but also on welding process heat efficiency, as illustrated in **Figure 10**.

It can be seen that the width of the top of the weld decreases with the increase of the gap width, subsequent increase in the gap width did not affect. The next increasing gap width did not have a strong influence on the weld metal width on the top plate. The width at the root of the weld and in the middle is increased by increasing the gap. As a result, the amount of filler metal is increased. Influence of slot width to the width of the weld is shown in **Figure 11**.

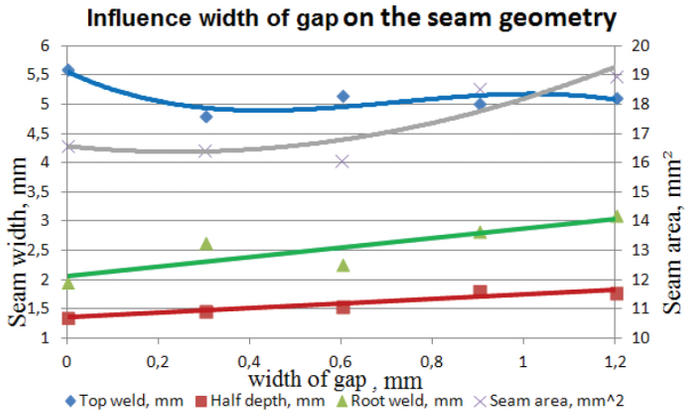

Figure 11. Influence of the gap width on the weld metal geometry.

It is also visible (**Figure 12**) that the optimum size of the gap is 1.2 mm. It can be explained that with increasing gap the welding pool width increases too, and, therefore, the volume of the dropping melting metal is higher. The reason for this is gravity.

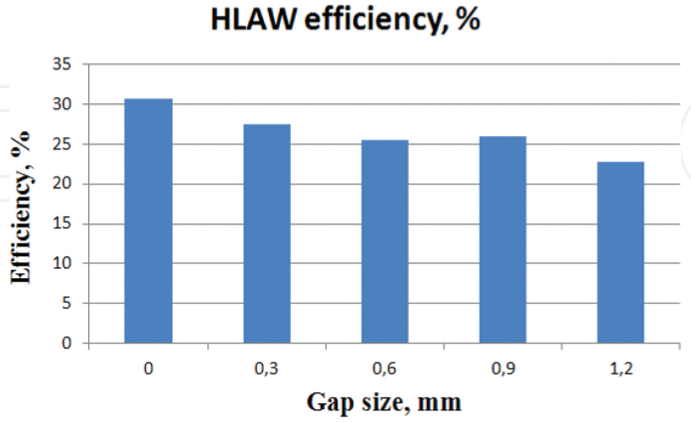

Figure 12. Influence of the gap width on the HLAW efficiency.

Analysis of the influence of the gap between the workpieces showed that its optimum size varies in the range of 0–0.3 mm. If a gap of 0.6–0.9 mm undercuts were observed, a gap width

of 1.2 m lack of filler material was also observed. The volume of the welding wire in the root and half depth of the weld increased simultaneously with increasing gap width. Also, increasing the gap width from 0 to 1.2 mm decreased HLAW efficiency from 30.6 to 22.7%. The results of the experiments described above allow to create a mathematical model for the prediction of the welded joint geometry at HLAW with gap. The integration of the model with the CAE system, LaserCAD [22], allows to predict the welded joint geometry at the HLAW with different gap widths.

Schematically the interaction of different physical processes that are important for processing HLAW is shown in **Figure 13**. Different tasks are connected through boundary conditions; when solution of one task determines boundary condition for another, as through direct influence of equation coefficients.

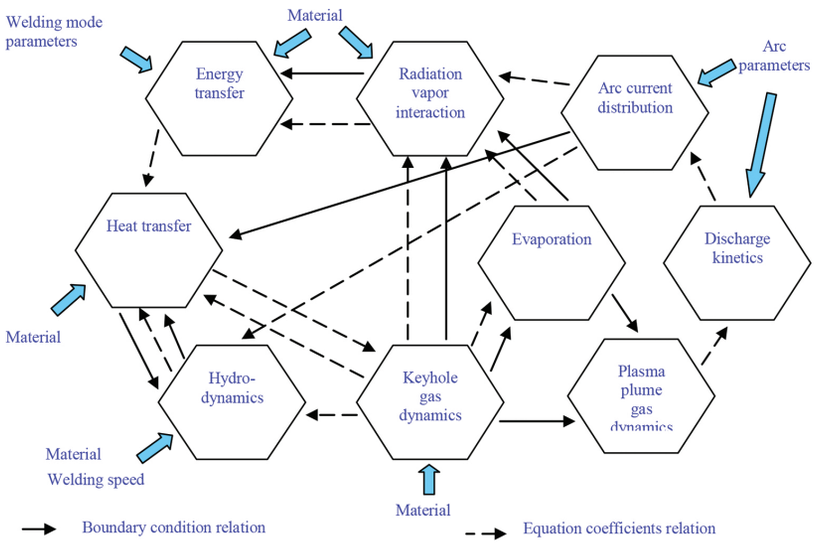

Figure 13. Structure of physical model of HLAW process.

Mathematical formulation of this physical model have been put on the basis of a number of steady-state process models, such as [23, 24], or [25], which allow to simulate a shape and size of melt pool as well as temperature distribution in weld bath and HAZ during hybrid HLAW welding.

For successful technology development it is also necessary to have a physical adequate description of melt pool dynamic behavior, which is responsible of formation of such welding defects as humping, porosity, spiking, and undercuts. This description has been designed on the basis of dynamic model of laser welding process [26]. The model is based on the formalism of Lagrange mechanics, which allow consider phenomena—wave motion of the cavity surface, change of the shape and sizes of the weld pool in time, and influence of the cavity motion as the whole on oscillations of its depth and radius.

The system of Lagrange equations for description of melt pool dynamic behavior can be represented as [27]:

http://dx.doi.org/10.5772/64522

$$\frac{\mathrm{d}}{\mathrm{dt}}\frac{\partial L}{\partial \dot{q}_i} - \frac{\partial L}{\partial q_i} = Q_i + R_i \,, \tag{2}$$

where q_i assumes H (depth of penetration, s_0 (keyhole cross-section area), $s_1,\ldots s_n$ (amplitudes of waves of different length), consecutively, Q_i is the generalized forces, and R_i is the dissipative function [27].

The mathematical formalism of solution of this system allows to carry out the dynamic analysis of occurrence of porosity and spiking, as shown in **Figure 14**.

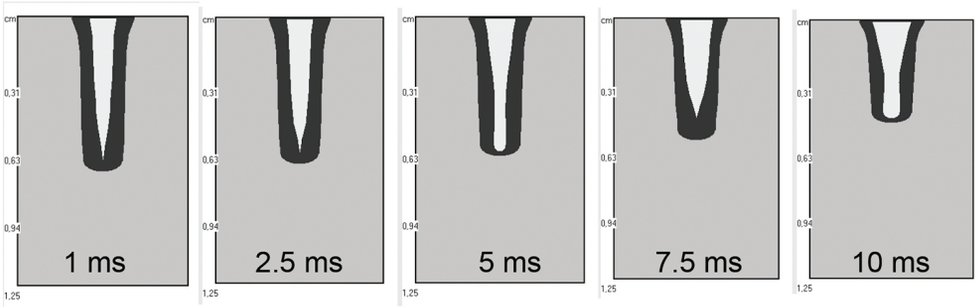

Figure 14. Simulation of the melt pool dynamics at HLAW, material – mild steel, laser beam power – 4.5 kW, welding speed – 12 mm/s, focal radius – 0.2 mm, focal distance – 30 cm, arc power – 2.5 kW.

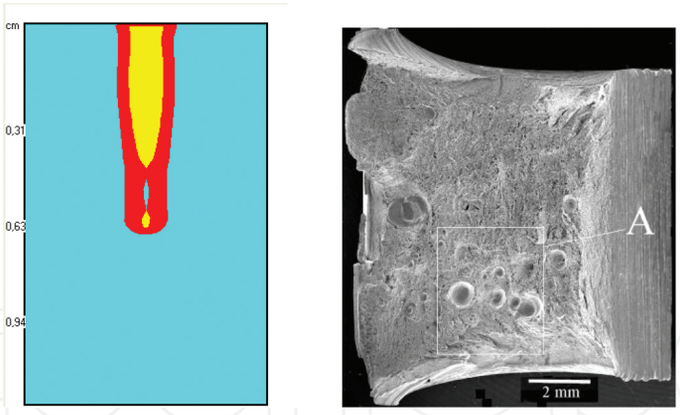

Figure 15. Simulation of porosity appearance due to cavity collapse (left) and results of experiment.

Analysis of the obtained results shows that dense occupation of the confined areas on the phase portraits by the phase trajectories explain the turbulent character of the cavity oscillations. It explains the calculation results independence for initial conditions. Sizes attractor is determined by the welding regimes.

The simulation results showed that hybrid welding of different generalized coordinates have different spectra of oscillations. The low frequencies below 100 Hz are equal to the radius of the cavity and the depth of the oscillation. Increasing the depth of penetration leads to a shear

rate range toward lower frequencies. Long (S_1) and short (S_2) waves have the highest frequency range to 10 kHz. These spectra also depend on the cavity depth. The increase of feeding velocity also decreases the low-frequency oscillations. The same approach can be used for analysis of porosity and spiking appearance (**Figure 15**).

3. Design of technological equipment for hybrid processes

The peculiarities of HLAW process lead to specific requirements for technological equipment for this process. Development of technological hybrid welding equipment is easier using the block-module approach. It allows inheritance in design and interoperability and also decreases development time. According to this approach, each installation includes laser power source, arc source, special welding tool, system of control, cooling system, gas distribution system, welding parts manipulator, seam tracking system, and process monitoring system. Joining of subsystem is provided by common interfaces for control, mechanic connecting, gases, and water. Using this approach, a number of machines have been designed for industry; some of these are described below.

First, technological installation, which we describe below in details, has been developed for hybrid laser-MAG welding of oil and gas pipes of large diameter (**Figure 16**). It provides welding of pipe steel with thickness of more than 12 mm together by one pass with a speed of up to 3 m/min. Simulation with LaserCAD allowed to determine parameters of installation for this purpose: laser source power is not less than 15 kW; beam diameter in focus is 0.3–0.4 mm; welding current is not less than 250 A; and diameter of the electrode wire is in range of 1–2 mm.

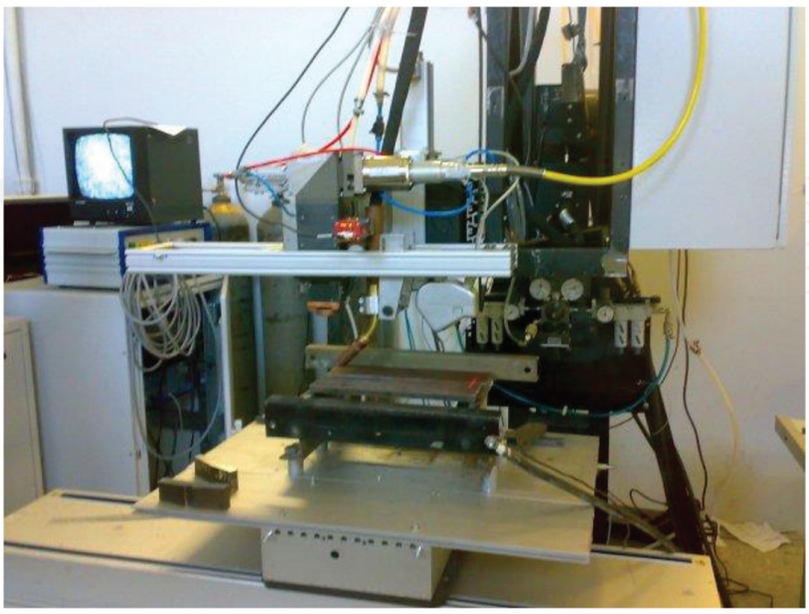

Figure 16. Hybrid welding equipment.

This hybrid laser-arc complex contains: IPG fiber laser LS-15, arc power source with current of up to 1500 A, and numerical control filler wire feeding equipment, special working tools, CNC module of preparation, and distribution of used gases, monitoring system of the welded joint, tracking system with scanner laser sensor, process monitoring system, and control system.

This module is used in complex welding of metallic workpieces with a possible gap of up to 2 mm, MAG torch is installed in front of the laser. This complex mainly includes positions already mentioned above.

Stabilization of the hybrid module position and control is described in more detail in [2]. Precision of keeping the focus point position of the laser head relative to welded blanks in the vertical direction is ±0.2 mm, and in the cross-section direction is ±0.5 mm.

The control system of hybrid laser-arc complex is developed as a hardware-software complex. Present system controls the components of the complex. The system includes a control subsystem forming welds subsystem monitoring and automatic control system.

It provides reading profile blanks geometry control, tracking the welding process at speeds of up to 6 m/min, the welding head positioning, control of the laser source, the control operation of the arc, and gas control system. The system also has a built-in protection against harmful conditions and operational control using the monitoring system.

Development of the control and monitoring systems for process of laser-arc welding is still a relevant task. Using of such systems is essential for the adoption of these technologies into the industry.

To solve this problem, it is necessary to carry out researches of the weld pool dynamics and also define basic mechanisms of defects formation specified for welding with deep penetration. For developing this system, secondary emission signals coming from laser-arc action zone were also analyzed and sensors for their registration were included.

The monitoring system, designed for HLAW, is based on registration of optical emission in different spectral ranges, depending on the range [5]. Sensors are installed in two directions and are equipped with a video camera. It simplifies the guidance process and allows tracing the spatial variation of the active zone. Synchronous registration, processing, and recording of signals are realized by using developed software.

Series of experiments on welding of model samples was carried out for verifying the monitoring system. Test results confirm the possibility of weld formation monitoring using the multisensor monitoring system (**Figure 17**). The presented results confirm the ability to monitor porosity level in weld using the developed system.

However, to use the monitoring system in real production it requires further research aimed at understanding the characteristics of particular process [28], identifying typical process defects, and adaptation monitoring system for this technological process.

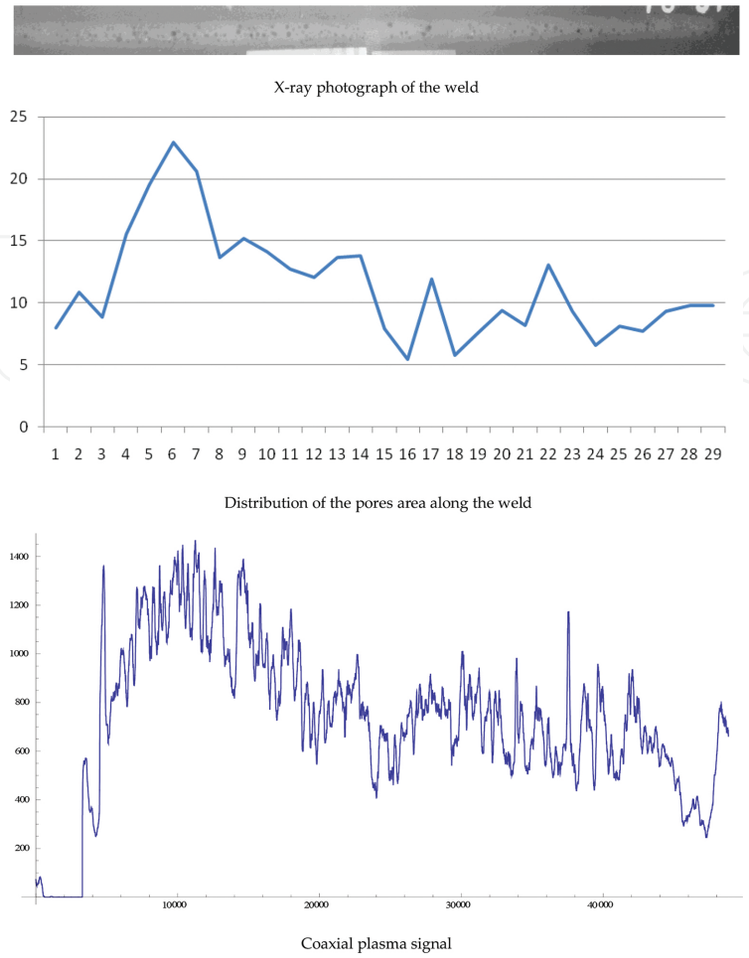

Figure 17. Signal response of the coaxial plasma sensor to change the level of porosity. X-ray photograph of the weld. Distribution of the pores area along the weld. Coaxial plasma signal.

For solving problems, the control system consists of several subsystems: laser control; arc equipment control; gas equipment control; welding head stationing; determination of the metal joint geometry; the control of parameters and protection of the laser welding head; the central controller module; and operating computer. For communication with other modules of the complex a card of CAN interface is put in the computer.

Other HLAW system [29], shown in **Figure 18**, based on soft direction belt, on which a motion unit with hybrid module, seam tracking, and filler wire feeding are mounted. Another subsystem is located in the stationary unit. In the equipment, 20 kW fiber laser with two direction switches is used. It allows to weld two joints in one time. This system uses a new inverter arc source. A used subsystem has a number of design features, for example, tracking sensor operating at high power in welding, and with a high degree of reflected radiation. However, they require special processing techniques of received signals [30]. Monitoring system for providing quality control process should capture the emergence of various defects (porosity, humping) [28]. The control system of this complex is implemented on the same base as the previous one.

Hybrid technology permits to create mobile technological equipment, which is able to perform all spectra of process advantages.

Control and stabilization of position of the hybrid laser-arc module relative to the joint is fulfilled by linear drives system installed on moving platform. It operates the same way as the stationary machine.

Figure 18. Mobile hybrid orbital system.

Another example of HLAW machine, based on the same design approach, is robot-based installation (**Figure 19**).

Figure 19. Robot-based HLAW machine on the base of 25 kW fiber laser.

Robot-based scheme of machine allows to weld parts of up to 4 m in length in different space positions.

4. Technology of HLAW

There are several fields of applications [31], in which usage of HLAW is especially prospective. First of them is production of large diameter pipes for oil and gas. The technology for different thickness of pipe walls was designed and the examples are shown in **Figure 20**.

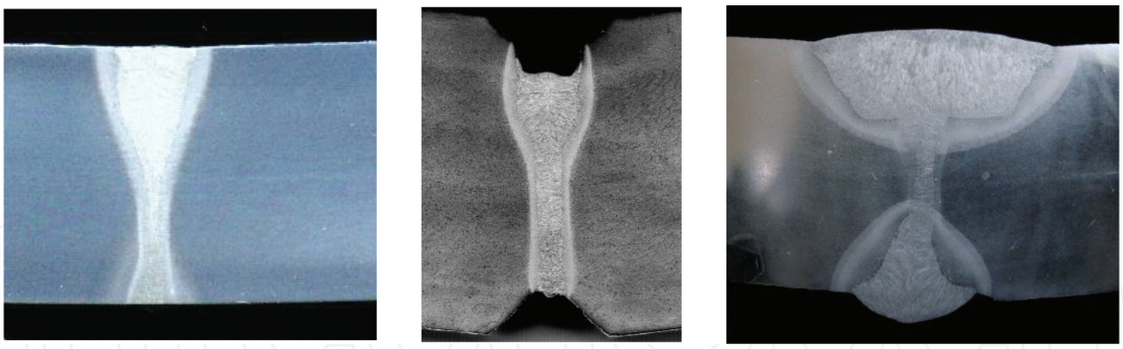

Figure 20. Macrosection of the one pass weld (left), three passes weld (center – first technological pass), right – technological pass and two filled passes by submerged arc welding. Depth is 15 mm left and 24 mm center and right. Material is steel X80.

Optimization of arc torch position relative to laser beam and optimization of composition of arc gas mixture together with usage of specially designed filler wire with ultrafine admixtures allow to avoid appearance of different defects, such as porosity, hot cracks, and humping. Also, it provides value of impact energy on temperature −40°C in the bounds of 140–200 J for pipe steel X80. HLAW also could be used for welding of nonturnable joints during pipeline building. In this case, hybrid scheme allows to increase not only the process productivity and joint quality but also process tolerance. Technology allows appropriate weld formation even in the case of more than 3 mm of vertical displacement of pipe joint edges (**Figure 21**).

Figure 21. Root pass side. Orbital pipeline hybrid welding with 2 mm gap and 3 mm vertical displacement.

Next prospective field of HLAW is shipbuilding [32]. Usage of this technology allows to increase dramatically the productivity of creation of flat sections for ship body. Because HLAW allows to get a weld with parallel walls displacement (**Figure 22**), it is possible to minimize welding stress and distortions, as shown in **Figure 23**.

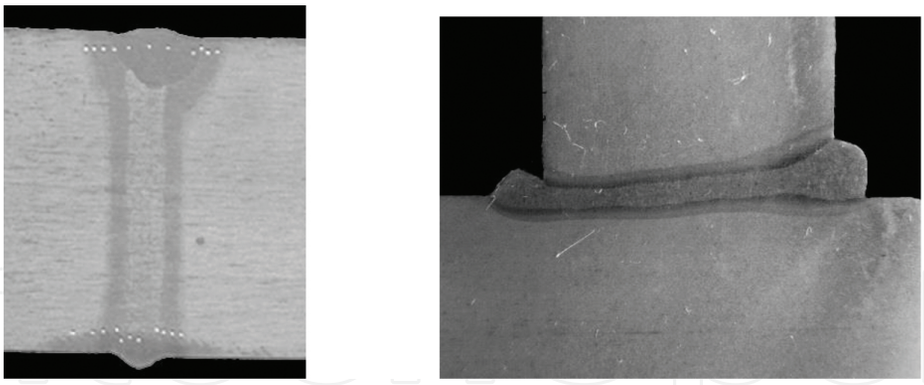

Figure 22. Butt HLAW joint in shipbuilding section (Material – steel PCE36, 20 mm thickness) – left, angle joint in shipbuilding section (Material – steel 09Г2С 15 mm thickness) – right.

Figure 23. Comparison of MAG welded ship body section (left) with HLAW case (right).

5. Peculiarity of metal structure formation in hybrid welding

To reduce the constructions weight new high-strength steels are applied. Characteristics of these steels are determined by parameters of ensembles of ultrafine inclusions. New technologies for car bodies are based on tailored blanks. Weight reduction without decreasing the strength is achieved by using high-strength steels and alloys in the production blanks. However, it is necessary to ensure satisfactory plastic weld characteristics.

This requires the use of welding technique, which provides the required level of ductility of weld seams and the same quality as laser welding process provides. Using a high-speed thermal cycling is the one of most promising techniques for getting good microstructure and mechanical properties [33]. This may be accomplished by welding two heat sources following one after another, for example, tandem laser welding [34]. However, from an economic standpoint it is advisable to use cheap local sources of heating as the second source, such as a powerful lamp.

To select treatment regimes, which provide the requisite microstructure and properties of the alloy, it is necessary to have a quantitative definition of the effect of temperature cycling on phase and structural transformations in the material. Modern concepts of phase transforma-

tions mechanisms under the laser exposure on Fe-based alloys [35], which became the basis of thermodynamics of phase transitions, do not take into account the nonequilibrium characteristics of fast transformation processes that result in the appearance of nonequilibrium microstructures in laser processing treatment. Thermodynamic characteristics do not allow to predict the temperature mutations for both transformations depending on the rate of heating and do not provide results for the nonstationary leak diffusion process. A quantitative description of the structural components is impossible without these factors. They can be formulated using only the kinetic theory of phase transformations, which has been made for the case of welding steels [36], and will be discussed in more detail in the example.

Phase transformations in Fe alloys under the beam treatment are defined as the metal structure consisting of two components. The first one is connected to decay (or formation) of solid solution of carbon in iron and formation (decay) of ferric carbide. The second process involves the conversion of FCC-BCC upon cooling after heating. A kinetic model was developed to determine the parameters of the formation and growth of the carbide inclusions.

The ratio between the surface area and the volume of the carbide inclusions depends on its shape. For the growth process, it can be considered as a point source. Concentration field around inclusion has a spherical symmetry. The inclusion can be considered as a sphere with an effective radius a. The nonequilibrium growth of new phase carbide inclusions is described using kinetic equation of the chemical reaction:

$$\frac{da}{dt} = K_1(T) \cdot C - K_2(T) \tag{3}$$

where $K_1(T)$ and $K_2(T)$ is a constant forward and reverse reactions, C is the carbon concentration on the surface of the inclusions, and T and t are the local temperature and time. The reaction speed constants are given by the Arrhenius formula:

$$K_{1,2}(T) = K_{1,2}{}^{(0)} \exp\left(U_{f,s} \Big/ kT \right), \tag{4}$$

where U_f, U_s are activation energy of the direct and reverse reaction, $K_1{}^{(0)}$, $K_2{}^{(0)}$ are frequency factors.

The superficial concentration is determined by a solution of the diffusion equation:

$$\frac{dC}{dt} = D\Delta C = D\frac{1}{r^2}\frac{\partial}{\partial r}\left(r^2 \frac{\partial C}{\partial r} \right) \tag{5}$$

The boundary condition on the surface of the growing inclusion (at $r = a$) is the condition of the solute flux continuity:

http://dx.doi.org/10.5772/64522

$$-D\left.\frac{\partial C}{\partial r}\right|_{r=a} = K_1(T)\cdot C\big|_{r=a} - K_2(T) \tag{6}$$

The admixture concentration far from the growing inclusion is determined by its average value C_0:

$$C\big|_{r\to\infty} \to C_0 \tag{7}$$

The solution of this problem has been obtained by standard methods of mathematical physics:

$$C = C_0 - \frac{1.56}{D\sqrt{\pi}}\frac{\left(K_1C_0 - K_2\right)}{\left(\frac{K_1}{D} - \frac{1}{a}\right)}. \tag{8}$$

Pay attention to the mutual influence in the carbide inclusions ensemble and having denoted the carbon concentration in the cementite as C′ (for Fe_3C C′ ≅ 0.25) and inclusion number density as n, the ensemble of spherical inclusions can be obtained as:

$$C_0 = C_0 - nC'\frac{4}{3}\pi a^3 . \tag{9}$$

To determine a value of the parameter n, it is possible to connect the n value with a solubility limit, which can be determined from the thermodynamic phase diagram. Having denoted the solubility limit as $C_{\lim}(T)$, one can get from a substance conservation condition:

$$n = \frac{C_0 - C_{\lim}(293)}{\frac{4}{3}\pi a_{\lim}^3 C'} \tag{10}$$

where $a_{\lim}$ is a limit size of the growing inclusion. Then the equation for inclusion radius can be rewritten as:

$$\frac{da}{dt} = K_1\left(C_0 - nC'\frac{4}{3}\pi a^3 - \frac{1.56}{\sqrt{\pi}D}\frac{K_1C_0 - K_2}{\frac{K_1}{D} - \frac{1}{a}}\right) - K_2 \tag{11}$$

Euler's method is used for solving the equations of growth of carbides. According to the results, $a_{\lim}$ should be included in the equation. Preliminary value of $a_{\lim}$ should be introduced, which

provides the same final value of the inclusion radius a. The values of parameters, used for calculation in this article for low carbon steel, are given by the next list: $K_1^{(0)} = 45$ m/s, $K_2^{(0)} = 2.2$ m/s, $U_f = 1.26 \cdot 10–19$ J/atom, $U_s = 1.60 \cdot 10^{-19}$ J/atom, $D_0 = 2 \cdot 10^{-6}$ m^2/s, $U_d = 1.38 \cdot 10^{-19}$ J/atom.

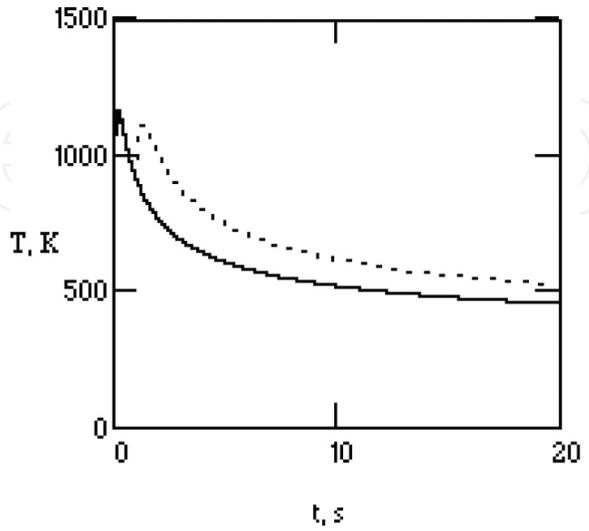

Figure 24. Temperature cycle for steel 08U (solid line – laser processing, dotted line – hybrid processing). Delay between temperature peaks 1 s.

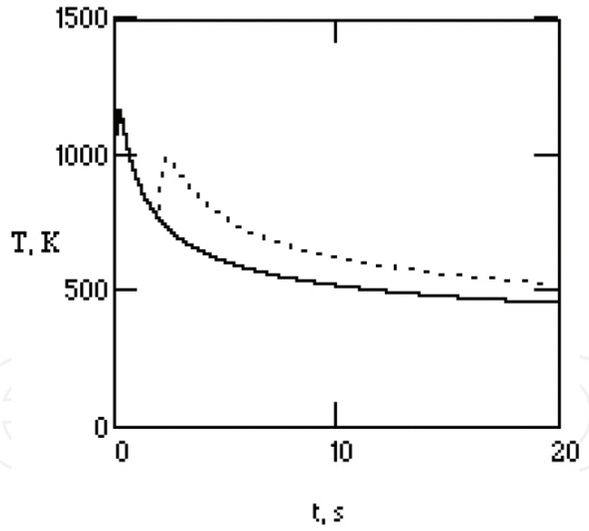

Figure 25. Temperature cycles for steel 08U (solid line – laser processing, dotted line – hybrid processing). Delay between temperature peaks 2 s.

Eventually, the kinetic model for the transformation $\alpha - \gamma$ should be formulated on the same principles as the model of nucleation and growth of inclusions. The interphase border movement rate in this case is that the diffusion Peclet number is not small, the diffusion equation, as against a problem about carbides growth, has been solved considering a convective term. On the other hand, since growing grain sizes are significantly greater than the

http://dx.doi.org/10.5772/64522

thickness of the diffusion layer, the problem is seen as univariate. Simultaneous solution of the related tasks about kinetics of new phase grains growth and the diffusion of carbon allow us to calculate the amount of a new phase at any point in the cycle. The result is a self-consistent system of equations, which describe material microstructure formation at the high-speed heating and cooling. The original structure adopted by the initial size of the carbide inclusions and initial grain sizes affect the diffusion coefficient. The thermal cycle is an input parameter, the parameters of which are determined by the technological cycle. The solution allows to calculate the evolution of the phase composition of the steel in the treatment zone.

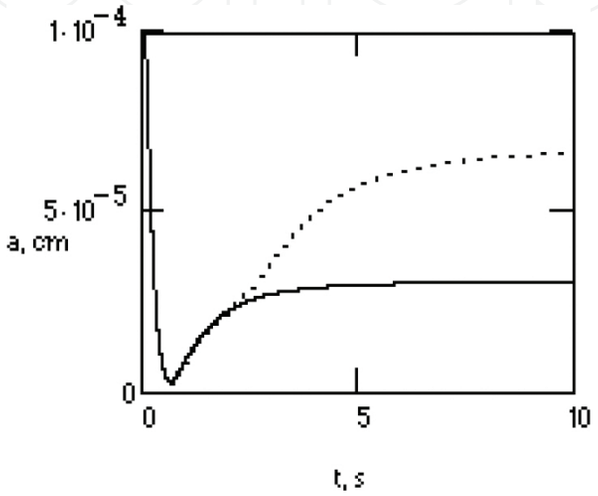

Figure 26. Calculation results for carbide nanoinclusions sizes for steel 08U (solid line – laser processing, dotted line – hybrid processing). Delay between temperature peaks 1 s.

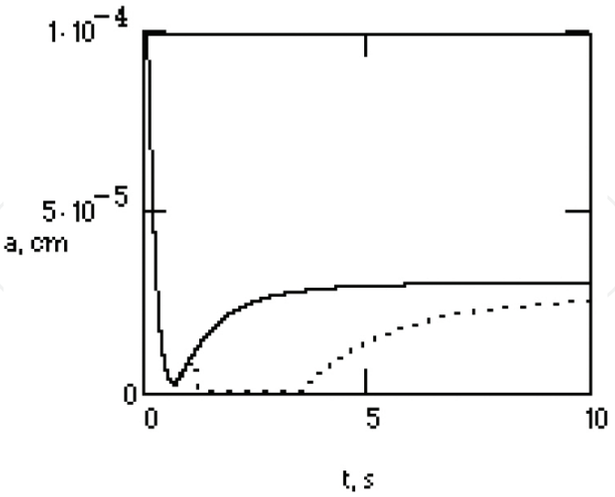

Figure 27. Calculation results for carbide nanoinclusions sizes for steel 08U (solid line – laser processing, dotted line – hybrid processing). Delay between temperature peaks 2 s.

Changing the form of a temperature cycle, which can be realized not only by HLAW, but also by another hybrid technologies, such as laser-light, dual beam, and others, it is possible to

achieve both size reduction and enlargement of the carbide inclusions in comparison with a temperature cycle, which is typical for laser action without an additional heat source (**Figures 24–29**).

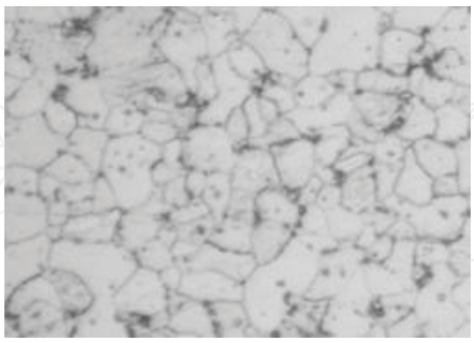

Figure 28. Microstructure after hybrid action, the maximal heating temperature is 1200 K, field width 50 μm. Delay between temperature peaks 1 s.

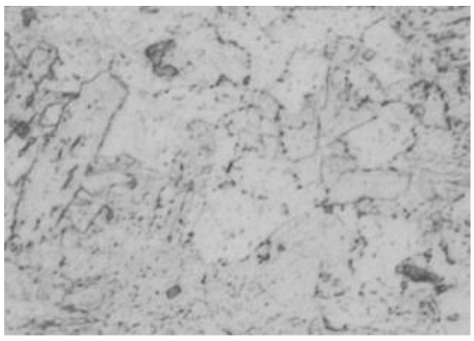

Figure 29. Microstructure after hybrid action, the maximal heating temperature is 1200 K, field width 50 μm. Delay between temperature peaks 2 s.

Influence of processing parameters for the delay between the first and second peaks of the cycle is shown in **Figures 24–29**. As obtained by theoretical studies, decrease in the time delay between the peaks results in a significant reduction in the size of carbide inclusions.

Microhardness distribution analysis showed that the welds obtained by hybrid welding have significantly less variation in the values of microhardness versus laser welding samples. Decrease of martensite part in weld metal allows raising its plasticity by more than 40%. So it can be concluded that hybrid welding technology suggests an additional possibility to control phase structure parameters in comparison with laser welding as it has been shown in the example of hybrid laser-light process.

As stated above, the carbides precipitation and nature of thermal cycles influence the process of phase composition formation. For estimation of steels phase composition, the time-temperature transformation diagrams of austenite decay together with curves corresponding to thermal cycles are usually used. The method of phase composition quantitative assessment based on Quench factor analysis was described in [37] and successfully tested on aluminum

http://dx.doi.org/10.5772/64522

alloys. Later on Quench factor analysis was applied for investigation possibility of predicting steel's mechanical properties during heat treatment [38], but in these works, processes of carbide formation and their influence on actual position of austenite decay C-curves were not considered. As was shown in [36], the nonequilibrium kinetics of new phase nucleus formation and nonstationary diffusion are influence by phase condition formation in practical welding conditions. Such point of view was used for logical design of quantity precipitate calculation for low-carbon steel welding, and realized as a computer program for the estimation of thermal field, which was used in the model described above. The calculation was carried out for steel 08U, the comparison of results and experimental data revealed their acceptable coincidence (**Figures 30** and **31**).

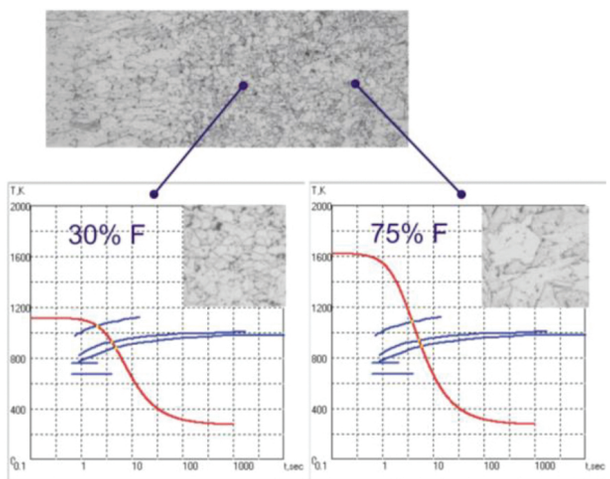

Figure 30. Comparison of calculation results of phase combination with experiment, low carbon steel 08U – laser frequency 5 Hz, pulse duration 7 ms, radiation power – 2.25 kW, lamp electric power – 5.16 kW, welding speed 2 m/s.

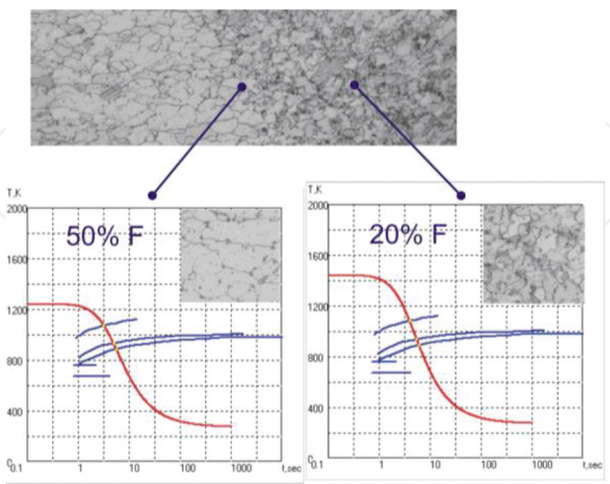

Figure 31. Comparison of calculation results for phase combination with experiment, low carbon steel 08U – laser frequency 10 Hz, pulse duration 3.5 ms, radiation power – 4.5 kW, lamp electric power – 5.726 kW, welding speed 4 mm/s.

Finally, it is possible to conclude that the use of hybrid welding instead of laser one allows to increase the melting efficiency and to provide stability of weld formation at welding metals in large variety of thickness. Also, hybrid welding technology provides additional possibility to control phase structure parameters, allowing to decrease the level of welding stress and distortion, and increasing welding productivity. Present level of technology development allows to design reliable and cost-effective technological equipment for hybrid laser-arc welding on the basis of high-power fiber lasers.

Author details

G. A. Turichin

Address all correspondence to: olgaklimova.ti@yandex.ru

Institute of Laser and Welding Technologies, Saint-Petersburg, Russian Federation

References

[1] W. M. Steen, Methods and apparatus for cutting, welding, drilling and surface treating. Patent 1547172 Great Britain, MKI V23K 26/00, 9/00, Publ. 06.06.79.

[2] F. O. Olsen, Hybrid laser arc welding, Woodhead Publishing, Denmark, 2009, 336 p.

[3] B. Ribic, T. A. Palmer and T. DebRoy, Problems and issues in laser-arc hybrid welding, International Materials Reviews, 2009, 54(4), 223–244.

[4] V. A. Lopota, Y. T. Sukhov and G. A. Turichin, Computer simulation of laser beam welding for technological applications, Izvestija Akademii Nauk, Ser. Phys, 1997, 61(8), 1613.

[5] G. A. Turichin, A. M. Grigor'ev, E. V. Zemlyakov, E. A. Valdaitseva, U. Dilthey and A. Gumeniuk, Special features of formation of plasma torch under conditions of hybrid laser-arc welding, High Temperature, 2006, 44(5), 647–655.

[6] M. Capitelli, A. Casavola, G. Colonna and A. De Giacomo, Laser-induced plasma expansion: theoretical and experimental aspects, Spectrochimica Acta Part B, 2004, 59, 271–289.

[7] D. F. Farson and K. R. Kim, Generation of optical and acoustic emissions in laser weld plumes, Journal of Applied Physics, 1999, 85(3), 1329–1336.

[8] L. J. Radziemski and D. A. Cremers, Laser-induced plasmas and applications, Dekker, New York, 1989, p. 336.

[9] T. X. Phuoc, An experimental and numerical study of laser-induced spark in air, Optics and Lasers in Engineering, 2005, 43, 113–129.

[10] L. G. Loitzynski, Mechanics of liquid and gas, Moscow, Drofa, 2003.

[11] K. Ramachandran et al., Structural analysis of converging jets in a triple torch plasma system, Journal of Physics D: Applied Physics, 2003, 36, 1198–1203.

[12] A. Revuelta et al., Confined axisymmetric laminar jets with large expansion ratios, Journal of Fluid Mechanics, 2002, 456, 319.

[13] V. Golant et al., Basis of plasma physics, Moscow, Atomizdat, 1977, 348 p.

[14] U. Diltey, A. Gumeniuk, V. Lopota and G. Turichin, Kinetic description of keyhole plasma in laser welding, Journal of Physics D, 2000, 33(21), 2747–2753.

[15] Y. Raizer, Laser spark and discharge propagation, Moscow, Science, 1974, 308 p.

[16] V. Lopota, G. Turichin, E. Valdaitseva, E. Pozdeeva and A. Gumeniuk, Computer system of electron beam and laser welding modeling, The Paton Welding Journal, 2006, 4, 29.

[17] G. Turichin, E. Pozdeeva and E. Zemlyakov, Numerical-analytical model of electrode wire melting in laser-arc welding, Physics and Chemistry of Material Processing, 2007, 4, 41-45./rus/.

[18] G. Turichin, I. Tzibulsky and M. Kuznetsov, Technology of laser-arc welding, Saint-Petersburg, Russia, Polytechnic University, 2015, 48 p.

[19] F. Kong, W. Liu, J. Ma and E. Levert, Feasibility study of laser welding assisted by filled wire for narrow-gap butt-jointed plates of high-strength steel. Welding in the World, 2013, 57, 693–699.

[20] 20. I. Tsibulskiy, M. Kuznetsov and A. Akhmetov, Effect of welding position and gap between samples on hybrid laser-arc welding efficiency, Applied Mechanics and Materials, 2014, 682, 35–40.

[21] M. Rethmeier, S. Gook and A. Gumenyuk, Perspectives of application of laser-GMA-hybrid girth welding for pipeline construction. Proc. of the 6 Int. Conf. "Beam Technology and Laser Aplication", Russia, Saint-Petersburg, 2009. pp. 278–288.

[22] G. Turichin, E. Valdaytseva and I. Tzibulsky, Computer analysis of beam material processing: LaserCAD simulation system, Photonics, 2008, 6, 18–21.

[23] E. Beyer, M. Dahmen, B. Fuerst, E. W. Kreutz, H. Nitchs, G. Turichin and W. Schulz, A tool for efficient laser processing, Proceedings of 14 Int. Congress on application of lasers – ICALEO-95, San Diego, USA.

[24] A. Kaplan, Influence of the beam profile formulation when modeling fiber-guided laser welding, Journal of Laser Applications, 2011, 23, 042005.

[25] G. Turichin, E. Valdaytseva, I. Tzibulsky, A. Lopota and O. Velichko, Simulation and technology of hybrid welding of thick steel parts with high power fiber laser, Physics Procedia, Proceedings of the 6th International WLT Conference on Lasers in Manufacturing, LiM" Munich, 2011. pp. 646–655.

[26] G. Turichin, E. Valdaitseva, E. Pozdeeva, U. Dilthey and A. Gumeniuk, Theoretical investigation of dynamic behavior of molten pool in laser and hybrid welding with deep penetration, Paton Welding Journal, 2008, 7, 11–15.

[27] V. A. Lopota, G. A. Turichin, I. A. Tzibulsky, E. A. Valdaytzeva, E.-W. Kreutz and W. Schulz, Theoretical description of dynamic phenomena in laser welding with deep penetration, Proceedings of SPIE – Proceedings of the 1998 6th International Conference on Industrial Lasers and Laser Applications, ILLA-98. Shatura, RUS, 1999. pp. 98–107.

[28] G. Turichin, E. Zemlyakov, K. Babkin and A. Kuznetsov, Monitoring of laser and hybrid welding of steels and Al-alloys, Physics Procedia, 2014, 56, 1232–1241.

[29] G. Turichin, O. Velichko, A. Kuznetsov, J. Pevzner, O. Grinin and M. Kuznetsov, Design of mobile hybrid laser-arc welding system on the base of 20 kw fiber laser, Proceedings – 2014 International Conference Laser Optics, LO, Saint-Petersburg, Russia, 2014. C. 6886481

[30] K. Babkin, E. Zemlyakov, G. Turichin and A. Kuznetsov, Use a technical vision in in automatic control of scanning laser welding, Nauchno-Technicheskie vedomosti SPbPU, 2015, 3(226), 142–149.

[31] G. Turichin, I. Tzibulsky, E. Valdaytseva and A. Lopota, Hybrid laser arc welding of metals of large thickness, Welding and Control (RUS), 2009, 3, 16–23.

[32] G. Turichin, I. Tzibulsky, V. Levshakov, N. Steshenkova and E. Valdaytseva, Laser and laser-arc welding of shipbuilding steels. Beam Technologies & Laser Application: Proc. of VII International scientific and technical Conference. Saint-Petersburg, 2013. pp. 90–103.

[33] E. L. Gyulikhandanov and A. D. Khaidorov, Effect of thermocycling on the structure and properties of high-speed steel obtained by electroslag remelting, Journal of Metal Science and Heat Treatment, 2002, 44(9–10), 426.

[34] C. Glumann, J. Rapp, F. Dausinger and H. Hugel, Welding with combination of two CO2 lasers — Advantages in processing and quality. ICALEO' 93, Orlando, FL, 1993, pp. 672–678.

[35] D. M. Gureev et al., Mechanisms of phase transformations in iron and steels at laser heating. Samara, Publishing House, Samara University, 1999.

[36] U. Dilthey, A. Gumenyuk and G. Turichin, Calculation of the kinetics of diffusion phase transformations in low-alloyed steels in beam welding, Paton Welding Journal, 2006, 2, 11–16.

[37] J. T. Staley, Quench factor analysis of aluminium alloys. Material Science and Technology, 1987, 3(11), 923–935.

[38] G. E. Totten, Y. H. Sun and C. E. Bates, Simplified property predictions AISI 4140 based on quench factor analysis. Third International Conference on Quenching and Control of Distortion, Prague, Czech Republic, 24–26 Mar. 1999. pp. 219–225.

IntechOpen

IntechOpen